GEOMETRIC CONSTRAINTS FOR THE TOPOLOGY OPTIMIZATION OF STRUCTURES MADE OF PRIMITIVES

Hollis A. Smith, Julián A. Norato

University of Connecticut
191 Auditorium Road
U-3139, Storrs, CT 06269, USA

ABSTRACT

This paper presents a topology optimization method for the design of 2- and 3-dimensional structures composed of bars in which the joining locations and the angles between adjacent bars can be controlled through optimization constraints. The topology optimization is performed using the geometry projection method, whereby the parametric description of the bars is smoothly mapped onto a fixed finite element mesh for analysis. By directly designing the geometric parameters of the bars as opposed to, for example, the element-wise densities or node- wise level set values of conventional topology optimization approaches, this method readily facilitates constraints on the geometry. This ability is leveraged in this work to impose a minimum angle between adjacent members, and to define regions of the geometry in which connections between components may be allowed or prevented so as to produce designs that are readily manufacturable. Even though these geometric constraints are presented in the context of the design with isotropic components, they can be readily extended to design with primitives made of anisotropic materials. The applicability of this methodology is demonstrated by several numerical examples.

1. INTRODUCTION

In recent years, topology optimization (TO) has become a standard engineering design tool due to its ability to generate novel structures that exhibit optimal performance. The most common and heavily researched TO technique is free-form density-based TO, which determines the optimal distribution of material within a specified design domain. In density-based TO, the design space is parameterized by a pseudo-density field ρ that is smoothly interpolated between 0 (void) and 1 (solid). This pseudo-density field is discretized using a fixed finite element (FE) mesh on which an ersatz material model is used for the analysis. The material in a given element is weighted by a function of the pseudo-density ρ, to effectively produce a weak (void) material when $\rho = 0$, or a reference solid material when $\rho = 1$. The pseudo-density $\rho \in [0,1]$ is modeled as a continuous variable, however intermediate values of ρ do not correspond to any physical material, so the 'solid isotropic material with penalization' (SIMP) model [1, 2] replaces ρ with a penalized density, typically using a power law. This penalization has the effect of making intermediate densities structurally inefficient, thus pushing the optimizer to render mostly 0 or 1 densities corresponding to a mostly solid-void design. The smooth ersatz-material model facilitates the sensitivity analysis of structural responses, thus enabling the use of efficient gradient-based optimization methods.

The other predominant type of TO techniques is the level-set method [3] [4], which represent the structural design implicitly via the zero level-set of a function, naturally inducing a solid/void

SAMPE Conference Proceedings. Charlotte, NC, May 20-23, 2019. Society for the Advancement of Material and Process Engineering – North America.

design. These methods also employ an ersatz material for the analysis, whereby an element density is computed from nodal values of the level-set function; or, they employ analysis techniques such as the extended finite element method (XFEM) that sharply capture the boundary. Level-set TO methods retain the advantage of ease of differentiation (enabling the use of gradient-based optimizers); however, this advantage comes at the expense of other challenges, such as relatively slower convergence (cf. [5]). On the other hand, level-set TO methods have the advantage of maintaining a mostly 0-1 design throughout the entire optimization, which is beneficial for certain types of problems.

The greatest strength of density and level-set TO methods is the ability to naturally accommodate changes in topology using a fixed mesh for the primal and sensitivity analyses. These techniques have thrived because of their ability to produce complex, organic shapes; however, these organic designs are often difficult to fabricate for the range of available materials, manufacturing techniques, and structural dimensions.

In response to the manufacturing challenges presented by the organic designs rendered by free-form TO, Norato et al. [6] formulated the geometry projection method in order to restrict the design space to a set of geometric primitives. In the geometry projection method, the design space is parameterized by a set of geometric variables (length, width, position, orientation, etc.), which are smoothly mapped to a pseudo-density field for the analysis, thus retaining two distinct advantages of density based TO: the ability to use a fixed analysis grid throughout the optimization, and the use of efficient gradient based optimization algorithms. Additionally, in the geometry projection method, the presence of a component itself is a design variable (achieved by ascribing a size variable to each component), thus allowing the optimizer to directly include or remove any component from the design. Along a similar vein, the method of Movable Morphable Components (MMC) was formulated by Guo et al. in [7] to parameterize the design space of a density based TO with geometric variables, however in the MMC, redundant components can be 'removed' from the design only by being engulfed in another component.

These geometric approaches to TO have the significant advantages over free-form techniques that they facilitate fabrication with stock material, have a direct translation to a computer-aided design (CAD) model, and can incorporate geometric considerations to facilitate manufacturing of the design. One of the major challenges with these methods in regards to manufacturability is that overlaps between primitives are not easy to manufacture, and highly acute angles between members may make them difficult to join in their fabrication.

This work considers imposing constraints that prevent primitive overlaps and acute angles between primitives that are difficult to manufacture. Other researchers have investigated the use of geometric constraints on geometric primitives in TO to improve manufacturability. For example, Hoang and Jang [8] formulated constraints for thickness control using variable thickness bars by ensuring a minimum void region outside a certain distance from each bar's medial axis, however, their formulation does not restrict the overlapping of members—this is in fact the only way for the optimizer to remove components from the design. Guo et al [9] formulated geometric constraints to control angles so as to produce designs for additive manufacturing that do not need supports. Zhang et al [10, 11] formulated a geometry projection scheme in which the geometric primitives which compose the generated structures are fixed-thickness plates. In [11], a constraint is imposed in the optimization problem that enforces a minimum separation-distance between plates to ensure tool access in the manufacturing; however, this method assumes a solid panel to which the plates attach as reinforcing ribs.

In this work, two geometric constraints are formulated in order to render designs that are more amenable to manufacture. The first constrains the minimum angle between bars. This constraint is unique in that it simultaneously considers the angle between members, as well as their proximity—thus allowing it to serve simultaneously as a constraint on the angle between nearby members, as well as to impose a minimum separation distance between parallel members. Second, a general geometric constraint is formulated in which portions of the geometric primitive can be specified as attachment-regions (which are allowed to intersect with other primitives); all other regions are restricted from overlapping other primitives. The boundary between the overlap and no-overlap regions is defined geometrically, and then projected smoothly onto the finite element grid as a smoothly differentiable field $\rho_{\text{overlap}} \in [0,1]$ to indicate 0 (non-overlappable elements) 1 (overlappable elements). To demonstrate the effectiveness of these constraints, several numerical examples are presented.

2. FORMULATION

2.1 Geometry Projection

The driving concept behind the geometry projection method is the smooth mapping from a high-level parametric design description onto a pseudo-density field. This projection of the geometry is achieved by considering a sampling window (a ball of radius r) at any point **x** in the design domain; the projected density is defined as the volume fraction of the sample window that intersects the solid structure ω:

$$\rho_{\text{proj}} = \frac{|B_{x}^{r} \cap \omega|}{|B_{x}^{r}|} \tag{1}$$

If the sample window radius r is small relative to the curvature of the structural boundary ∂ω, then one can reasonably approximate this intersection everywhere as a circular segment in 2-dimensions, or a spherical cap in 3-dimensions. Given the signed distance d (along the outward normal) from the surface of the structural boundary to the point **x**, the projected density may be computed as

$$\rho_{\text{proj}}(d;r) = \begin{cases} 0, & \text{if } d \geq r \\ 1, & \text{if } d \leq -r \\ \dfrac{1}{\pi}\left(\pi - \arccos\left(\dfrac{d}{r}\right) + \dfrac{d}{r}\sqrt{1-\left(\dfrac{d}{r}\right)^{2}}\right), & \text{if } |d| < r \text{ in } 2-\text{dimensions} \\ \dfrac{1}{4}\left(\dfrac{d}{r}+1\right)^{2}\left(\dfrac{d}{r}-2\right), & \text{if } |d| < r \text{ in } 3-\text{dimensions} \end{cases} \tag{2}$$

In this work, the parameterization formulated in [6] for the offset surface of a line segment (circular-ended bars in 2-dimensions, spherical-ended bars in 3 dimensions) is employed to define the geometric primitives. Each bar b in the full set of bars $\mathcal{B}$ is parameterized by the two endpoints of its medial-segment $\boldsymbol{x}_{\text{sb}}$, $s \in \{1,2\}$, $b \in \mathcal{B}$, as well as the offset r_b (half the width), and a size variable $\alpha_b \in [0,1]$, which allows the corresponding bar to be included ($\alpha_b = 1$) or excluded ($\alpha_b = 0$) from the design. Since intermediate values of α_b have no physical meaning, the size variables are penalized in the spirit of SIMP so that intermediate values are structurally inefficient, pushing the optimizer to render designs that either include or exclude a given bar. The set of design variables for a single bar b may be expressed as $\boldsymbol{z}_b$ in equation (3), and the full set of design variables is $\boldsymbol{Z}_b = \{\boldsymbol{z}_b\} \; \forall b \in \mathcal{B}$.

$$\boldsymbol{z}_b = \begin{Bmatrix} \boldsymbol{x}_{1b} \\ \boldsymbol{x}_{2b} \\ r_b \\ \alpha_b \end{Bmatrix} \tag{3}$$

The signed distance for the offset surface of a segment may be expressed as a single function of its endpoints and its offset $\mathrm{d_b}(\mathbf{x}_{\mathrm{sb}}, \mathrm{r_b})$. This equation is omitted for brevity, and the reader is referred to [6] for the full derivation and its sensitivity.

Having obtained the signed distance as a function of the geometric design variables, the geometry projection is performed on the centroids $\mathbf{x}_\mathrm{e}$ of each element e in the finite element mesh to obtain a projected density ρ_{be} for each bar onto each element. The projected densities are penalized by weighting them with the penalized size variable $\breve{\alpha}_\mathrm{b} = \mathrm{penal}(\alpha_\mathrm{b}; \mathrm{p})$ as in equation (4) The penalization scheme used here is the SIMP interpolation, with $\mathrm{p} = 3$.

$$\breve{\rho}_{be} = \breve{\alpha}_b \rho_{be} \tag{4}$$

Then, penalized element densities are computed by taking the Boolean union over the full set of bars as described in [6], and are used to weight the solid material elastic tensor to compute the structural response using the finite element method.

2.2 Angle Constraint

It is desirable to prescribe a minimum angle between bars to facilitate the generation of designs made of bars that may be manufactured via traditional methods such as welding or fastening. However, the angle between bars should only be restricted when the bars come in close proximity to each other. The constraint on the angle between nearby bars is formulated as follows. Consider the unit normal along the bar medial segment from point $\mathbf{x}_{1\mathrm{b}} \rightarrow \mathbf{x}_{2\mathrm{b}}$ as given by equation (5)

$$\widehat{\boldsymbol{n}}_b = \frac{\boldsymbol{x}_{2b} - \boldsymbol{x}_{1b}}{\|\boldsymbol{x}_{2b} - \boldsymbol{x}_{1b}\|} \tag{5}$$

Then the cosine of the angle between bars b and b' is

$$c_{bb'} = \widehat{\boldsymbol{n}}_b \cdot \widehat{\boldsymbol{n}}_{b'} \tag{6}$$

And the angle between bars b and b' is determined depending on the side s of bar b and side s' of bar b' as $\theta_{\mathrm{ss'bb'}} \in [0, \pi]$.

$$\theta_{ss'bb'} = \begin{cases} \arccos c_{bb'}, & \text{if } s = s' \\ \pi - \arccos c_{bb'}, & \text{otherwise} \end{cases} \tag{7}$$

Figure 1 depicts the unit normals of bars $b = 1, b' = 2$ arranged in a parallelogram such that all 2^2 configurations of paired endpoints can be visualized. For example, when side 1 of both bars are at the same point ($\boldsymbol{x}_{1b} = \boldsymbol{x}_{1b'}$), then the angle between bars is in the lower left of the parallelogram ($\theta_{11bb'}$). The angles corresponding to the 4 possible pairings of the sides of any two bars $s, s' \in \{1,2\}$ are computed, and subsequently this is reduced to the set of angles that are too acute and occur between bars that are close enough, as prescribed by two parameters, θ^* and δ.

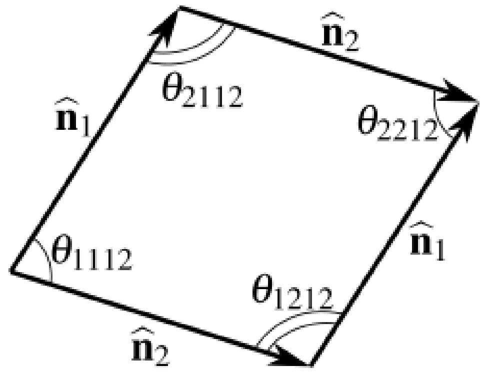

Figure 1: Parallelogram depicting angles between two bars

In order to constrain the angle between nearby bars to a minimum angle θ^*, first restrict the consideration to pairs of bars whose angles are below this value, i.e., when they are in violation of the constraint. To achieve this end, employ the regularized Heaviside (or sigmoid) function as defined in equation (8) to compute weights ρ_θ according to equation (9). The term ρ_θ serves to smoothly indicate the extent to which angles between bars should be considered ($\rho_\theta = 1$) or ignored ($\rho_\theta = 0$).

$$\widetilde{H}(x) = \frac{1}{2}\left(1 + \mathrm{erf}\frac{3x}{\sqrt{2}}\right) \tag{8}$$

$$(\rho_\theta)_{ss'bb'} = \begin{cases} 0, & \text{if } b = b' \\ \widetilde{H}\left(\dfrac{\theta^* - \theta_{ss'bb'}}{\varepsilon} - 1\right), & \text{otherwise} \end{cases} \tag{9}$$

In equation (9), $\varepsilon \in (0, \pi/4]$ is the parameter used to control the steepness of the smooth angle-indicator $(\rho_\theta)_{ss'bb'}$. Note that ρ_θ is explicitly set to zero for the zero-angle between a bar and itself. In this work, $\varepsilon = \pi/32$. Figure 2 depicts the distribution of ρ_θ for a pair of bars, and a given θ^*. As is illustrated in the figure, all angles larger than $\theta^*$are effectively ignored.

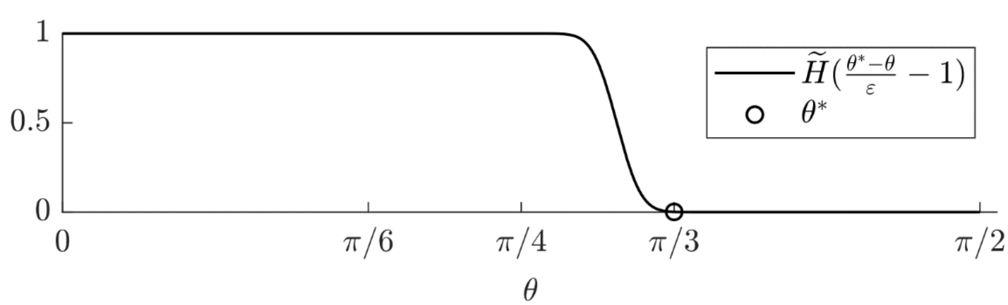

Figure 2: Smooth angle indicator ρ_θ for a pair of bars. $\theta^* = \pi/3, \varepsilon = \pi/32$.

Next, further restrict the consideration to angles between bars that are close. This is achieved by evaluating the distance $d_{sbb'}$ from the medial segment of bar b' to the endpoints $\boldsymbol{x}_{sb}$ of bar b.

$$d_{sbb'} = \begin{cases} \|\boldsymbol{b}_{sbb'}\|, & \text{if } \widehat{\boldsymbol{n}}_b \cdot \boldsymbol{b}_{sbb'} < 0 \text{ (left)} \\ \|\boldsymbol{e}_{sbb'}\|, & \text{if } \widehat{\boldsymbol{n}}_b \cdot \boldsymbol{e}_{sbb'} > 0 \text{ (right)} \\ \|\boldsymbol{g}_{sbb'}\|, & \text{otherwise (center)} \end{cases} \tag{10}$$

where

$$\begin{aligned} \boldsymbol{b}_{sbb'} &= \boldsymbol{x}_{sb} - \boldsymbol{x}_{1b'} \\ \boldsymbol{e}_{sbb'} &= \boldsymbol{x}_{sb} - \boldsymbol{x}_{2b'} \\ \boldsymbol{g}_{sbb'} &= \boldsymbol{b}_{sbb'} - (\widehat{\boldsymbol{n}}_{b'} \cdot \boldsymbol{b}_{sbb'})\,\widehat{\boldsymbol{n}}_{b'} \end{aligned}$$

To limit this field to nearby bars, a smooth Heaviside is employed which achieves a field that is effectively zero when the ends of bar b have separation of at least δ from bar b':

$$(\rho_{\text{dist}})_{sbb'} = \widetilde{H}\left(1 - \frac{d_{sbb'}}{(r_b + r_{b'} + \delta)/2}\right) \tag{11}$$

The smooth distance indicator ρ_{dist} allows one to restrict the consideration to pairs of bars in which either of the two ends s comes into close proximity of another bar. However, each pair of bars has 2 unique angles (cf. Figure 1) in four configurations depending on the pairing of endpoints. In order to limit the angle between the bars according to how they are physically positioned, the space is partitioned into three regimes based on the medial segment of bar b' as depicted in Figure 3 and also corresponding to the three branches of equation (10). When $\widehat{\boldsymbol{n}}_b \cdot \boldsymbol{b}_{sbb'} > 0$, limit $\theta_{s1bb'}$, and when $\widehat{\boldsymbol{n}}_b \cdot \boldsymbol{e}_{sbb'} < 0$, limit $\theta_{s2bb'}$. However, this discrete constraint is not differentiable, and so it is relaxed by using a smooth Heaviside:

$$(\rho_{s'=1})_{sbb'} = \begin{cases} 0, & \text{if } b = b' \\ \widetilde{H}\left(\dfrac{2}{r_b}\widehat{\boldsymbol{n}}_b \cdot \boldsymbol{b}_{sbb'} - 1\right), & \text{otherwise} \end{cases} \tag{12}$$

$$(\rho_{s'=2})_{sbb'} = \begin{cases} 0, & \text{if } b = b' \\ \widetilde{H}\left(-\dfrac{2}{r_b}\widehat{\boldsymbol{n}}_b \cdot \boldsymbol{e}_{sbb'} - 1\right), & \text{otherwise} \end{cases} \tag{13}$$

Equations (12) and (13) define the smooth indicator $(\rho_{s'})_{sbb'}$ that is zero when point $\boldsymbol{x}_{sb}$ is not on the same side (left or right) as $\boldsymbol{x}_{s'b'}$, and positive otherwise.

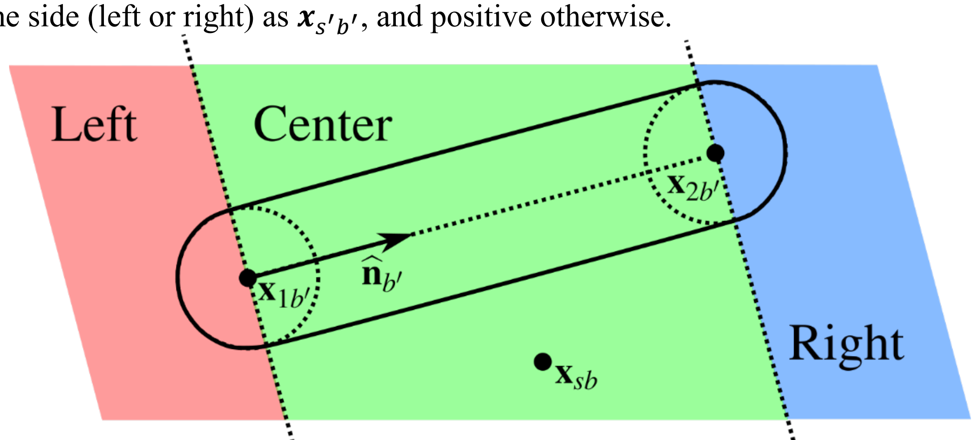

Figure 3: Partitions used to define if $\boldsymbol{x}_{sb}$ is to the left, center, or right of bar b'

Next, the smooth indicators ρ_θ and $\rho_{s'}$ are combined to define the angle indicator ρ_{angle} as

$$\left(\rho_{\text{angle}}\right)_{sbb'} = \sum_{s'} (\rho_{s'})_{sbb'} \, (\rho_{\theta})_{ss'bb'} \tag{14}$$

This is weighted by ρ_{dist} and the penalized size variables $\breve{\alpha}_{\text{b}}, \breve{\alpha}_{\text{b}'}$ and summed in order to form a single angle constraint g_{angle} as

$$g_{\text{angle}}(\boldsymbol{Z}; \theta^*, \delta) = \frac{1}{n_{\text{bar}}^2} \sum_{s,b,b'} \breve{\alpha}_b \breve{\alpha}_{b'} \left(\rho_{\text{angle}}\right)_{sbb'} (\rho_{\text{dist}})_{sbb'} \tag{15}$$

where n_{bar} is the number of bars in the design.

The angle constraint takes the current design $\boldsymbol{Z}$ along with the user-defined parameters θ^* and δ to compute a net violation of the constraint that is always nonnegative. This is an equality constraint ($g_{\text{angle}} = 0$), however this is relaxed by imposing a small upper limit $\varepsilon_{\text{angle}} \ll 1$ which specifies the net allowable violation of the constraint so it may be implemented as an inequality constraint $g_{\text{angle}} \leq \varepsilon_{\text{angle}}$.

One notable feature of this angle constraint is that it is purely geometric; there is no projection onto the finite element mesh to facilitate its computation. This results in a computation time and accuracy that is completely irrelevant of the quality or complexity of the finite element discretization. The constraint is also relatively inexpensive to compute for designs with a moderate number of bars since its time complexity is $\mathcal{O}(n_{\text{bar}}^2)$. The design sensitivity of this constraint may be computed readily via direct differentiation, however, it is also efficient, $\mathcal{O}(n_{\text{bar}}^3)$, to use finite differences to compute the sensitivity.

2.3 Overlap Constraint

It is often the case that components used to design structures have certain regions which should be used to join components. In this section, a constraint is formulated that can be applied to any geometric primitive on which certain regions are prescribed as attachment zones, here this constraint is applied to the ends of the bars as an example, cf. Figure 4.

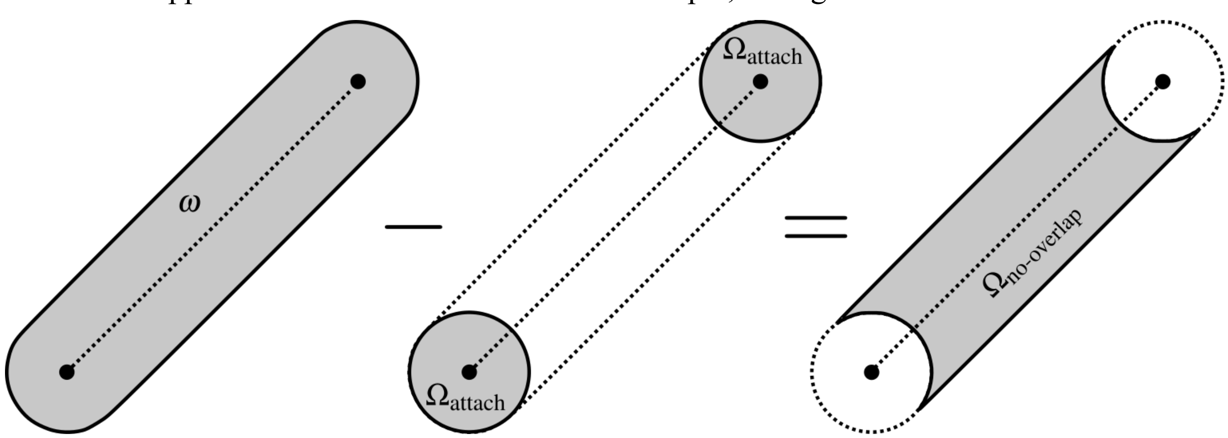

Figure 4: Domain of the primitive ω, regions specified for attachment Ω_{attach}, and regions where overlap is to be constrained $\Omega_{\text{no-overlap}}$.

First, the allowable-overlap (attachment) regions of each primitive are defined. One can use Boolean operations to define this region, or can define the region explicitly. In this work, the attachment region, Ω_{attach}, is explicitly defined as the spherical ends of the bars as illustrated in Figure 4. The union of the attachment regions over all bars is used to define regions in the design domain in which primitives are allowed to overlap. When computing the constraint, only overlaps inside the no-overlap region (the Boolean difference of the design domain and the attachment region) are considered to be in violation of the constraint. The effect of this approach is that the ends of bars may arbitrarily attach to any other part of the structure.

Then the geometry projection method is used to map the no-overlap regions onto the finite element mesh. The signed distance function used to project the no-overlap regions is computed using a smooth approximation for the maximum function according to equation (16). Here, the over-estimating Kreisselmeier-Steinhauser [12] function is used to approximate the maximum as expressed in equation (17). The accuracy of the approximation of the maximum improves with larger p at the cost of increased non-linearity. For the examples in this work $p = 8$.

$$(d_{\text{ends}})_e = \widetilde{\max}_{s,b}(r_b - \|\boldsymbol{x}_e - \boldsymbol{x}_{sb}\|; p) \tag{16}$$

$$\widetilde{\max}_i(x_i; p) = \frac{1}{p}\log\sum_i \exp(px_i) \tag{17}$$

After performing the geometry projection, an element-wise pseudo-density $\left(\rho_{\text{no-overlap}}\right)_e$ is obtained which vanishes inside the attachment regions, is unity in the no-overlap region and varies smoothly across the boundary $\partial\Omega_{\text{no-overlap}}$. The projected densities for each component are summed and weighted by this factor. The effect is to eliminate all terms that are in the allowable-overlap region, such that only the terms in the regions where overlaps are not allowed contribute to the constraint. The result is an element-wise value that should not exceed 1 for a valid design, and is everywhere positive. A relaxed conditional operation is applied to zero out all values that are smaller than one, and to only count the number of bars greater than one that are projected into the non-overlap region. Here, one can use the size-variable weighted "effective" density, or just the projected density directly. The effect of including the size variable is to allow the optimizer to remove bars in order to satisfy the overlap constraint in addition to moving them, but this also allows overlapping bars with intermediate size variables to satisfy the constraint—often rendering designs that do not converge to 0-1—thus the examples in this work do not include the size variable in the overlap constraint. The number of bars more than one that is projected into an element in the no-overlap region is approximated as $\tilde{n}_e$ in equation (18).

$$\tilde{n}_e = \widetilde{\max}_i(x_{ei}; p) - 1, \qquad x_{ei} = \begin{cases} 1, & \text{if } i = 1 \\ \sum_b \rho_{be}\left(\rho_{\text{no-overlap}}\right)_e, & \text{if } i = 2 \end{cases} \tag{18}$$

A value if $\tilde{n}_e$ that satisfies the overlap constraint should be everywhere zero (an equality constraint) but one can set an upper bound $\varepsilon_{\text{overlap}}$ on the volume of overlapping material and render the constraint's scale independent of the mesh resolution by weighting this element-wise value by the element volumes v_e and summing over the elements to aggregate the constraint:

$$g_{\text{overlap}}(\boldsymbol{Z}) = \sum_e \tilde{n}_e v_e \tag{19}$$

2.4 Optimization Problem and Implementation

The base optimization problem is to minimize the structural compliance subject to a volume fraction constraint. In addition, either or both of the angle and overlap constraints are imposed. The complete optimization problem is formally stated in Equation (20). The design sensitivities of the compliance and volume fraction are derived in [6], and the sensitivities for the angle and overlap constraints are omitted for brevity, but may be directly and readily derived. To demonstrate the effectiveness of the angle and overlap constraints to allow the optimizer to generate designs that improve manufacturability, two design problems are presented: a cantilever beam, and an MBB beam as depicted in Figure 5.

$$
\begin{aligned}
&\text{objective:} \\
&\qquad \min_{\boldsymbol{Z}} c = \boldsymbol{U}^{\top}\boldsymbol{F} \\
&\text{subject to:} \\
&\qquad \frac{\sum_e v_e \rho_e}{\sum_e v_e} \leq v^* \\
&\qquad g_{\text{angle}} \leq \varepsilon_{\text{angle}}, \qquad \text{if considering angle constraint} \\
&\qquad g_{\text{overlap}} \leq \varepsilon_{\text{overlap}}, \qquad \text{if considering overlap constraint}
\end{aligned}
\tag{20}
$$

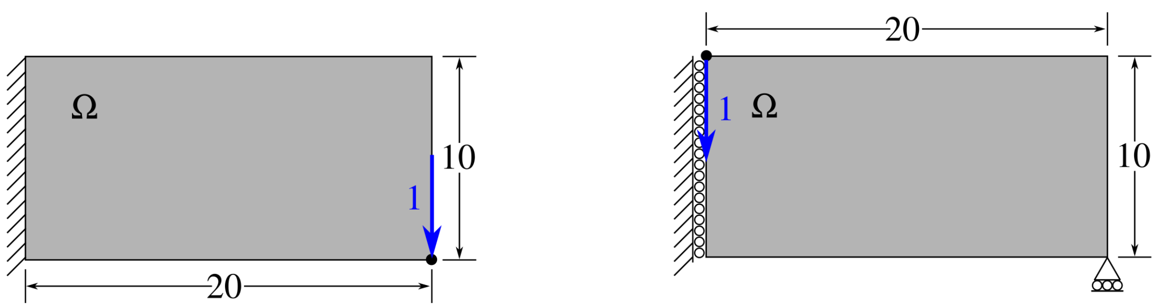

(a) (b)

Figure 5: Diagrams depicting the design domain Ω, and boundary conditions for the (a) cantilever beam and (b) MBB beam design problems.

The initial design consists of an array of 8 disconnected, equally-spaced, small bars with a radius of $r_b = 0.25$ and size variable of $\alpha_b = 0.5$ as depicted in Figure 6. To avoid an ill-posed analysis, the minimum density is chosen to be $\rho_{\min} = 10^{-2}$, so that the void region is interpolated as a material two orders of magnitude weaker than the solid material. The solid material is defined to have a unit Young's modulus, $E = 1$, and a Poisson ratio of $\nu = 0.3$.

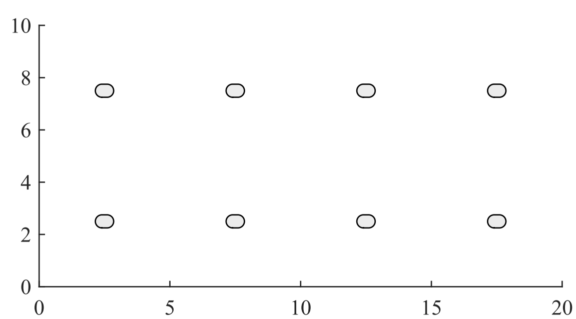

Figure 6: Initial design

The analysis is computed in MATLAB using linear, 4-node quadrilateral finite elements and the optimization problem is solved using the Method of Moving Asymptotes (MMA) [13].

3. RESULTS

3.1 Cantilever Beam

As a base-line, the case of a fixed bar-radius of $r_b = 0.25$ and only the volume fraction constraint with a target volume fraction of $v^* = 0.25$ is considered. The resulting design, depicted in Figure 7, has may parallel adjacent members which effectively act together as thicker members. The projected density field corresponding to this design is plotted in part (b) of the figure with the overlapping elements highlighted in red. The largest overlapping regions occur on the top and bottom of the left (fixed) edge where the long edge of these bars overlap. Any overlaps in the design would require cuts in order to fit the bars together, and cuts along the longitudinal edge of the bars are especially difficult and costly to make.

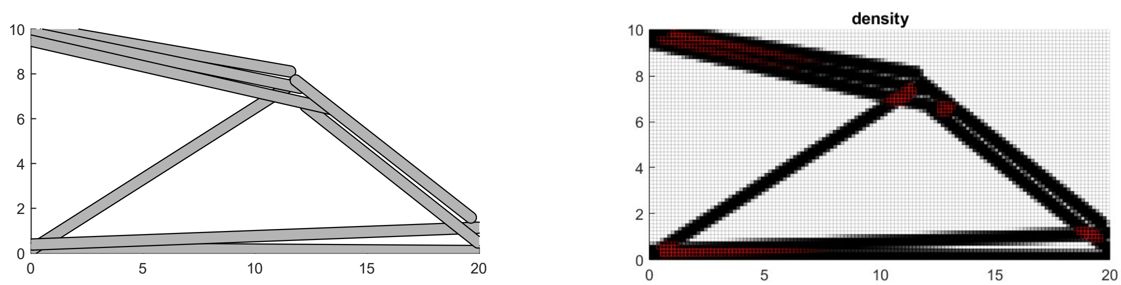

(a) (b)

Figure 7: Cantilever beam: $r_b = 0.25$, $v^* = 0.25$: (compliance = 1.291). (a) optimal design, (b) projected density (overlap highlighted in red).

Next, consider the addition of the angle constraint with a separation distance of $\delta = 1$. The separation distance is the smallest distance allowed between parallel bars. When the ends of any bar come within δ of another bar, then the minimum angle between those bars, $\theta^* = 30°$, is enforced by the constraint. The resulting design is depicted in Figure 8. One immediately notices the absence of the parallel adjacent bars seen the design without the constraint on the angle, as well as the fact that the voids between bars have opened up to allow more access for the joining of members.

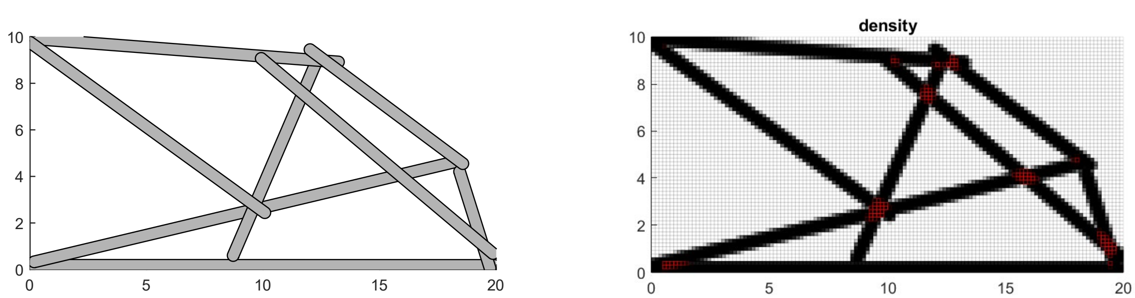

(a) (b)

Figure 8: Cantilever beam: $r_b = 0.25$, $v^* = 0.25$, $\theta^* = 30°, \delta = 1$, $,\varepsilon_{\text{angle}} = 10^{-3}$: (compliance = 1.552). (a) optimal design, (b) projected density.

If the gaps between bars are not large enough, one can increase the separation parameter δ. The design depicted in Figure 9 was obtained by setting $\delta = 4$. As expected, the two nearly parallel pairs of bars in the double 'X' shaped reinforcement that is generated in this structure are each separated by more than 4 units of distance.

Imposing the overlap constraint in addition to the angle constraint of the previous example yields the design depicted in Figure 10 with the 'M' shaped reinforcement and an inactive volume fraction constraint with a design volume fraction of 0.21.

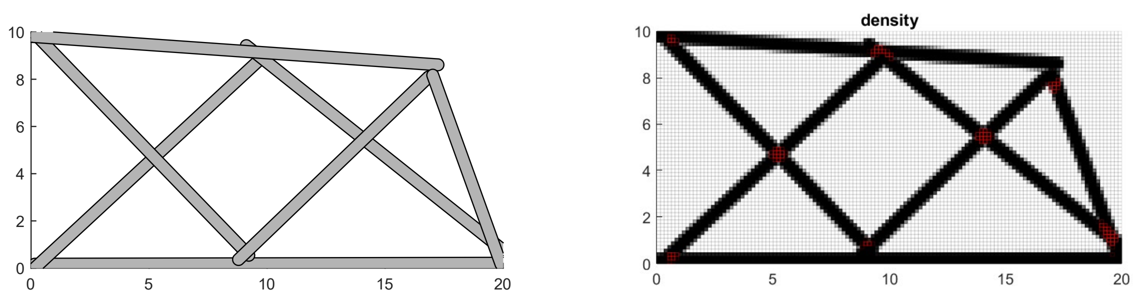

(a) (b)

Figure 9: Cantilever beam: $r_b = 0.25$, $v^* = 0.25$, $\theta^* = 30°$, $\delta = 4$, $\varepsilon_{angle} = 10^{-3}$: (compliance = 1.65). (a) optimal design, (b) projected density

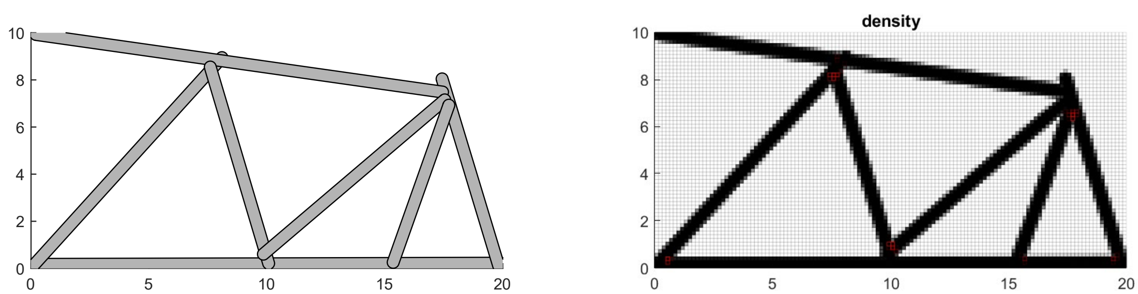

(a) (b)

Figure 10: Cantilever beam: $r_b = 0.25$, $v^* = 0.25$, $\theta^* = 30°$, $\delta = 4$, $\varepsilon_{\text{angle}} = 10^{-3}$, $\varepsilon_{\text{overlap}} = 10^{-4}$: (compliance = 2.065). (a) optimal design, (b) projected density.

In each of the previous examples, the compliance of the structure increased as the design space was further constrained, but this is not always the case. By allowing the radius of each bar to vary as $r_b \in [0.25, 1.25]$ with just the volume fraction constraint, the initial design in Figure 6 is very prone to falling into a local minimum—the '>' shaped structure depicted in Figure 11(a). When the angle and overlap constraints are imposed on this design, it was observed that these constraints not only rendered a design that is more manufacturable, but also helped to find a better local optimum from the same initial design (cf. Figure 12). This behavior is most likely due to the effect of the constraints to move overlapping members apart and to different angles, thus resulting in a greater chance of more internal members when the constraints are imposed.

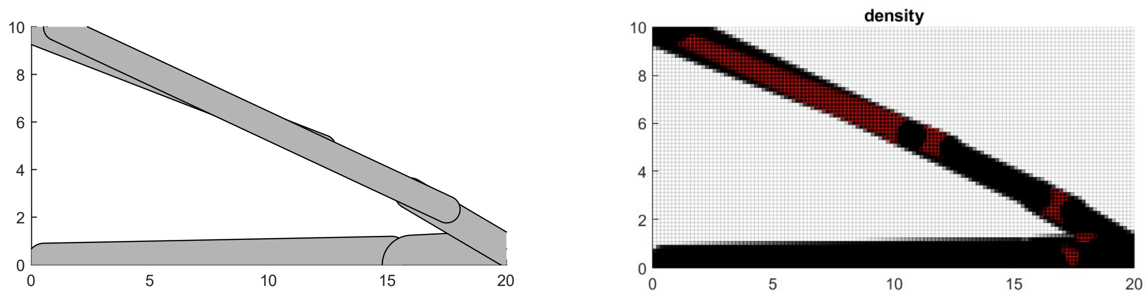

(a) (b)

Figure 11: Cantilever beam: $r_b \in [0.25,1.25]$, $v^* = 0.25$: (compliance = 1.531). (a) optimal design, (b) projected density.

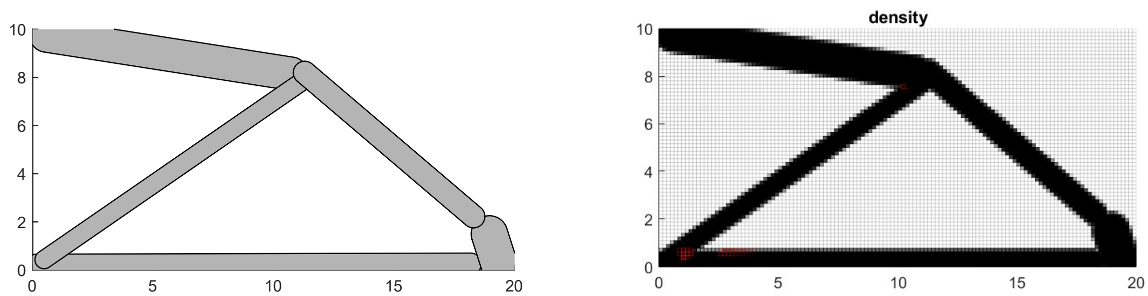

(a) (b)

Figure 12: Cantilever beam: $r_b \in [0.25,1.25]$, $v^* = 0.25$, $\theta^* = 30°$, $\delta = 4$, $\varepsilon_{\text{angle}} = 10^{-3}$, and $\varepsilon_{\text{overlap}} = 10^{-4}$: (compliance = 1.276). (a) optimal design, (b) projected density

3.2 MBB Beam

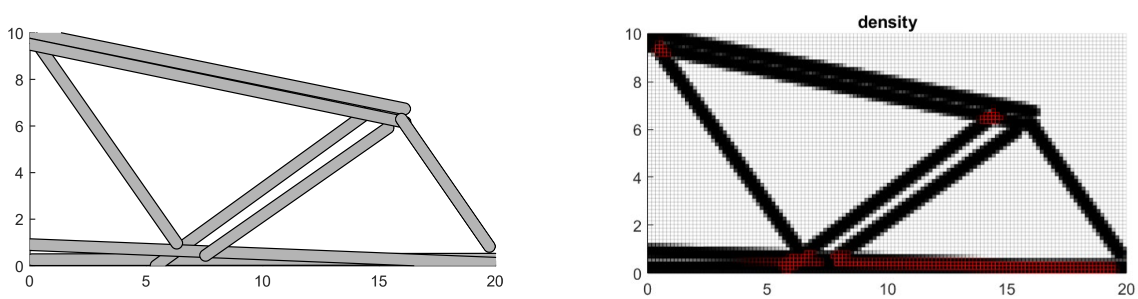

(a) (b)

Figure 13: MBB beam: $r_b = 0.25$ and only volume fraction constraint, $v^* = 0.25$: (compliance = 1.451). (a) optimal design, (b) projected density

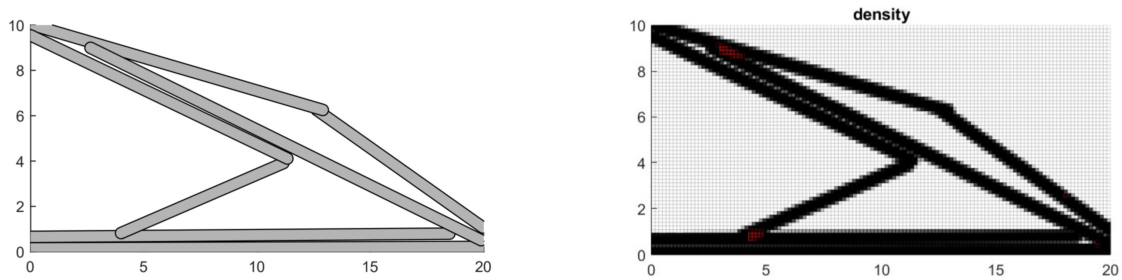

(a) (b)

Figure 14: MBB beam: $r_b = 0.25$, $v^* = 0.25$, and overlap constraint with $\varepsilon_{\text{overlap}} = 10^{-4}$: (compliance = 1.700). (a) optimal design, (b) projected density

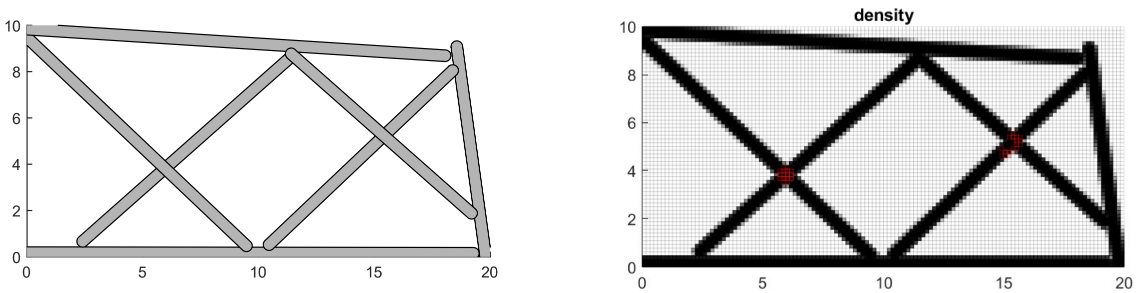

(a) (b)

Figure 15: MBB beam: $r_b = 0.25$, $v^* = 0.25$, $\theta^* = 30°$, $\delta = 4, \varepsilon_{\text{angle}} = 10^{-3}$, and overlap constraint $\varepsilon_{\text{overlap}} = 10^{-4}$: (compliance = 1.980). (a) optimal design, (b) projected density.

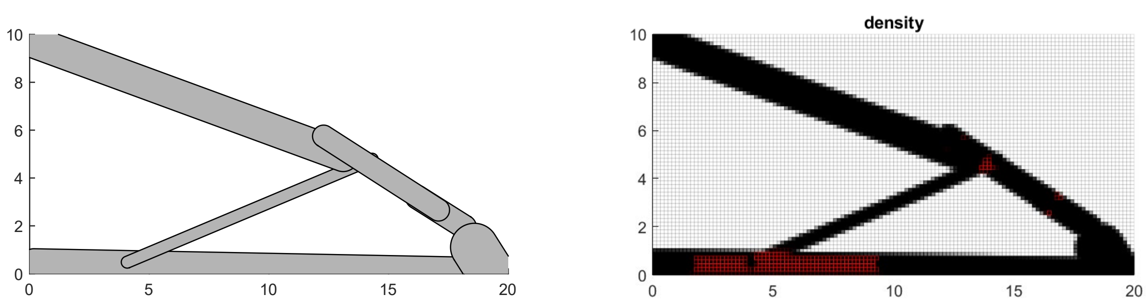

(a) (b)

Figure 16: MBB beam: $r_b \in [0.25,1.25]$, and only volume fraction constraint $v^* = 0.25$: (compliance = 1.554). (a) optimal design, (b) projected density

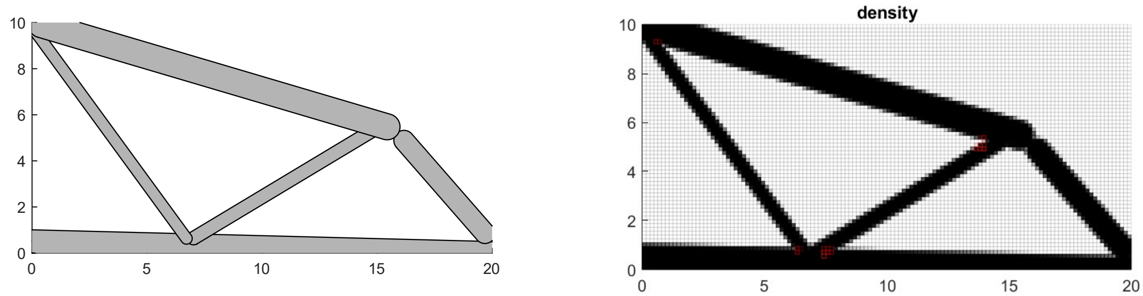

(a) (b)

Figure 17: MBB beam: $r_b \in [0.25,1.25]$, $v^* = 0.25$, $\theta^* = 30°$, $\delta = 4, \varepsilon_{\text{angle}} = 10^{-3}$, and $\varepsilon_{\text{overlap}} = 10^{-4}$: (compliance = 1.608). (a) optimal design, (b) projected density.

4. CONCLUSIONS

This work presented a topology optimization method for the design of structures composed of bars in which the joining locations and the angles between adjacent bars can be controlled through optimization constraints. A constraint on the minimum angle between nearby members that is completely geometric was imposed by leveraging the ability of the geometry projection method to perform topology optimization while directly designing the geometric parameters of the bars, and hence does not rely on the finite element mesh for its computation. The effectiveness of the angle constraint to allow the user to impose a minimum angle between nearby members, and also to impose a minimum separation distance between parallel members in the structure was demonstrated. This work also successfully formulates a constraint in which connections between components may be allowed or prevented so as to produce designs that are readily manufacturable. It was found that the imposition of these constraints typically produces designs with more internal structural members than designs in which components are allowed to freely overlap. Although these constraints are intended to increase manufacturability of generated designs at the cost of some structural performance, it was demonstrated that these constraints can, in some cases, help the optimizer to find a better local optimum. Although these geometric constraints have been presented in the context of design with isotropic bars, they are independent of the material model, and can be readily extended to design with primitives made of anisotropic materials.

5. REFERENCES

1. Bendsøe, Martin P. Sigmund Ole. *Topology optimization: theory, methods, and applications*. Springer Science & Business Media, 2013. https://doi.org/10.1007/978-3-662-05086-6

2. Bendsøe, Martin P. Sigmund Ole. "Material interpolation schemes in topology optimization." *Archive of applied mechanics*, 69(9-10) (1999): 635–654. https://doi.org/10.1007/s004190050248

3. Wang, Michael Y. Wang, Xiaoming. Guo, Dongming. "A level set method for structural topology optimization." *Computer methods in applied mechanics and engineering*, 192(1-2) (2003): 227–246. https://doi.org/10.1016/S0045-7825(02)00559-5

4. Allaire, Grégoire. Gournay, Frédéric D. Jouve, François. Toader, A-M. "Structural optimization using topological and shape sensitivity via a level set method." *Control and*

cybernetics, 34(1) (2005): 59. http://oxygene.ibspan.waw.pl:3000/contents/export?filename=2005-1-03_allaire_et_al.pdf

5. Van Dijk, Nico P. Maute K. Langelaar, M. Van Keulen, F. "Level-set methods for structural topology optimization: a review." *Structural and Multidisciplinary Optimization*, 48(3) (2013): 437–472. https://doi.org/10.1007/s00158-013-0912-y
6. Norato, JA. Bell, BK. Tortorelli, DA. "A geometry projection method for continuum-based topology optimization with discrete elements." *Computer Methods in Applied Mechanics and Engineering*, 293 (2015): 306–327. https://doi.org/10.1016/j.cma.2015.05.005
7. Guo, Xu. Zhang, Weisheng. Zhong, Wenliang. "Doing topology optimization explicitly and geometrically—a new moving morphable components based framework." *Journal of Applied Mechanics*, 81(8) (2014): 08100. https://doi.org/10.1115/1.4027609
8. Hoang, Van-Nam. Jang, Gang-Won. "Topology optimization using moving morphable bars for versatile thickness control." *Computer Methods in Applied Mechanics and Engineering*, 317 (2017): 153–173. https://doi.org/10.1016/j.cma.2016.12.004
9. Guo, Xu. Zhou, Jianhua. Zhang, Weisheng. Du, Zongliang. Liu, Chang. Liu, Ying. "Self-supporting structure design in additive manufacturing through explicit topology optimization." *Computer Methods in Applied Mechanics and Engineering*, 323 (2017): 27–63. https://doi.org/10.1016/j.cma.2017.05.003
10. Zhang, Shanglong. Norato, Julián A. Gain, Arun L. Lyu, Naesung. "A geometry projection method for the topology optimization of plate structures." *Structural and Multidisciplinary Optimization*, 54(5) (2016): 1173–1190. https://doi.org/10.1007/s00158-016-1466-6
11. Zhang, Shanglong. Norato, Julián A. "Optimal design of panel reinforcements with ribs made of plates." *Journal of Mechanical Design*, 139(8) (2017): 081403. https://doi.org/10.1115/1.4036999
12. G Kreisselmeier and R Steinhauser. *Systematic control design by optimizing a vector performance index in computer aided design of control systems*, pages 113–117. Elsevier, 1980. https://doi.org/10.1016/B978-0-08-024488-4.50022-X
13. Svanberg, Krister. "The method of moving asymptotes—a new method for structural optimization." *International journal for numerical methods in engineering*, 24(2) (1987): 359–373. https://doi.org/10.1002/nme.1620240207